

PROCEEDINGS OF SPIE

[SPIDigitalLibrary.org/conference-proceedings-of-spie](https://spiedigitallibrary.org/conference-proceedings-of-spie)

Directionality of A_0 Lamb wave mode scattering at defects

P. Fromme

P. Fromme, "Directionality of A_0 Lamb wave mode scattering at defects," Proc. SPIE 10170, Health Monitoring of Structural and Biological Systems 2017, 101701N (5 April 2017); doi: 10.1117/12.2260030

SPIE.

Event: SPIE Smart Structures and Materials + Nondestructive Evaluation and Health Monitoring, 2017, Portland, Oregon, United States

Directionality of A_0 Lamb Wave Mode Scattering at Defects

P. Fromme

Department of Mechanical Engineering, University College London, WC1E 7JE, UK

ABSTRACT

Localized and distributed guided ultrasonic waves array systems offer an efficient way for the structural health monitoring for large structures. The detection sensitivity for fatigue cracks depends on the orientation of the crack relative to the location of the sensor elements. Crack-like defects have a directionality pattern of the scattered field depending on the angle of the incident wave relative to the defect orientation and on the ratio of the defect depth and length to the wavelength. From FE simulations it has been shown that for cracks and notches almost no energy is scattered in certain directions from the defect, i.e., the data processing algorithm must take into account that for some transducer combinations no change in the signal even for a significant defect will be detected. The scattered wave field directionality pattern for an incident low frequency A_0 Lamb wave mode was predicted from 3D Finite Element simulations and verified from experimental measurements at machined part-through and through-thickness notches using a laser interferometer. Good agreement was found and the directionality pattern can be predicted accurately. The amplitude of the scattered wave is quantified for a systematic variation of the angle of the incident wave relative to the defect orientation, the defect depth, and the ratio of the characteristic defect size to the wavelength. Based on these results the detection sensitivity for crack-like defects in plate structures using guided wave sensors arrays can be quantified.

Keywords: Guided Ultrasonic Waves, Scattering, Crack

1. INTRODUCTION

For ageing aircraft, consisting of metallic components connected by fasteners, fatigue crack growth at locations of stress concentration constitutes a significant maintenance problem. A requirement exists for the nondestructive testing (NDT) of these structures to detect fatigue cracks before they have reached a critical length. Ultrasonic-based structural health monitoring (SHM) methods have been developed for the monitoring of cracks at fastener holes using an angle beam through transmission technique [1]. However, bulk wave ultrasonic testing (UT) often involves manual or automated scanning and necessitates local access to the inspected part [2]. Guided ultrasonic waves can achieve long propagation distances in thin structures, providing an efficient SHM methodology for large structures [3, 4]. High frequency guided waves have been employed to monitor fatigue crack growth at fastener holes [5-7] and to detect defects in multi-layered metallic structures [8]. For plate structures, localized [9] and distributed array systems using low-frequency guided ultrasonic waves have been developed for the detection of defects [10-12]. Advanced signal processing, e.g. minimum variance imaging taking the scattering pattern into account, has been shown to improve the sensitivity for crack-like defects and to allow for the estimation of the defect orientation [13].

The scattering of the A_0 Lamb wave mode at thickness changes in a plate has been studied in a 2D configuration [14]. Analytical and numerical models exist for the scattering of the A_0 mode at circular through holes, verified from experiments [15, 16]. Models and FE simulations predict the scattering at part-thickness circular defects [17]. The scattering of the A_0 Lamb wave mode at a fatigue crack emanating from a fastener hole has been reported previously [18]. Continuing from previous contributions [19], the directionality pattern of the A_0 Lamb wave mode scattering at notches in a plate has been investigated. The influence of geometrical parameters, such as the defect length and depth and the angle of the incident wave relative to the notch orientation was predicted from Finite Element (FE) simulations and measured experimentally. The obtained scattering characteristics are discussed with a view towards the detection of crack-like defects using guided ultrasonic waves.

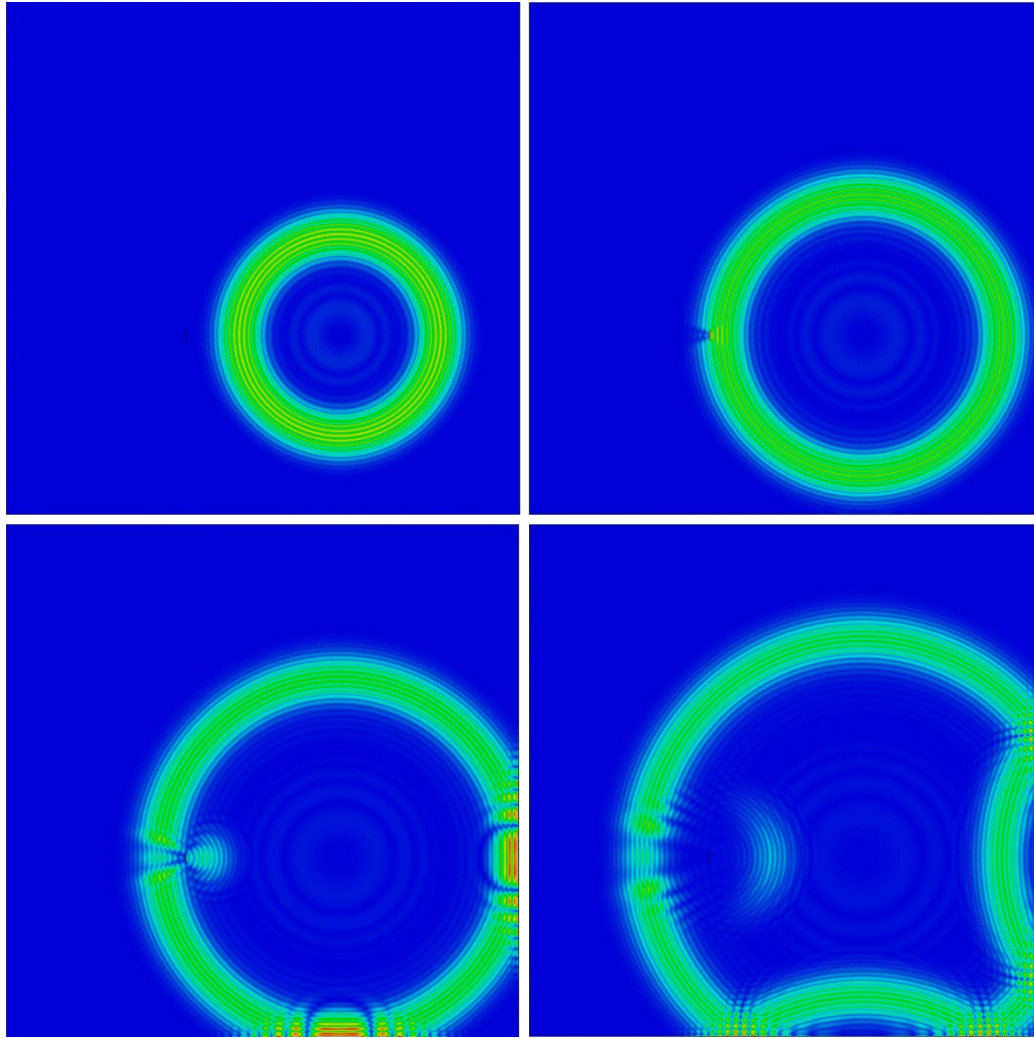


Fig. 1. Time snapshots of FE plate simulation, top view; $f = 100$ kHz; $\lambda = 19$ mm; $a = 20$ mm; wave crest propagating radially outwards from excitation point, wave scattered at notch with shadow effect and back-scattered wave visible.

2. FINITE ELEMENT SIMULATIONS

The scattering of the A_0 Lamb wave mode was simulated using three-dimensional (3D) Finite Element (FE) models with linear brick elements in ABAQUS Explicit (Fig. 1). The model of a 5 mm thick aluminum plate (size: 1 m x 1 m) with a notch of varying length and depth was implemented, similar to the model described in [19]. Explicit time integration was used, and the element size and time step were chosen to adhere to the usual stability criteria. Point excitation of the A_0 Lamb wave mode was introduced at chosen node locations 300 mm from the defect location, allowing for a variation of the incidence angle between 0° and 90° , relative to the normal of the notch. The excitation pulse was set as a 5 cycle toneburst with a center frequency of 100 kHz, corresponding to a wavelength λ for the A_0 mode of 19 mm. The out-of-plane displacement at the center (mid-plane) node on points in a square area around the defect was recorded. The time trace at each monitoring node was time gated to remove reflections from the plate edges. Fast Fourier Transform (FFT) was used to extract the complex magnitude (amplitude and phase information) at the center frequency of 100 kHz for each monitoring node. This captures the combined wave field of the incident wave and scattered wave. Additional simulations without a defect (pristine plate) were run to capture the incident wave field only. Taking the difference between the complex magnitudes for each point with and without a defect, the amplitude of the wave scattered at the defect can be isolated [16]. The amplitude of the scattered wave was extracted on a radius of 30 mm by interpolating between monitoring nodes to obtain an amplitude value every 5 degree. The methodology is described in detail in a previous contribution [19].

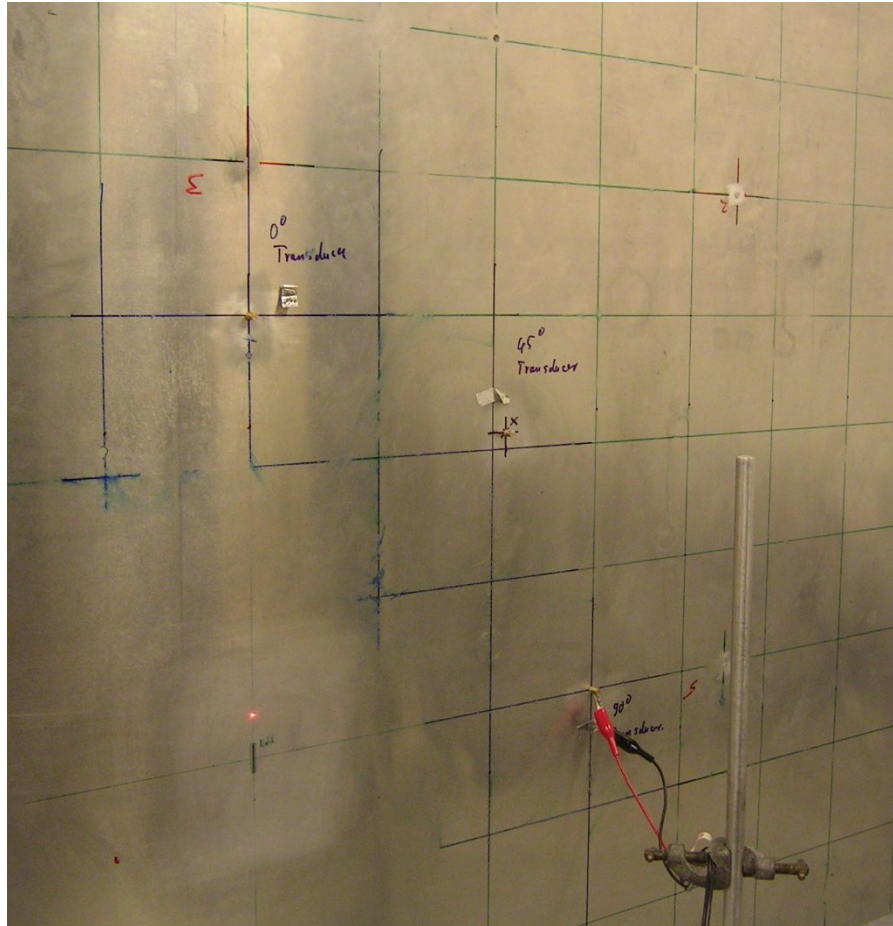


Fig. 2. View of experimental setup: aluminum plate (size: 1.5 m x 1 m) with 20 mm notch, 3 excitation transducers at 0°, 45°, and 90°, 300 mm from notch, and red laser interferometer measurement spot close to defect.

3. EXPERIMENTS

The scattered wave field around notches of 5 mm and 20 mm length was measured on a large, 5mm thick aluminum plate (size: 1.5 m x 1 m). The notches (width: 1 mm) were milled in four steps to give a varying depth of $\frac{1}{4}$, $\frac{1}{2}$, $\frac{3}{4}$, and through thickness. The notches had rounded edges due to the milling tool (diameter 1 mm) and a flat bottom for the part-through depths. Three excitation transducers were placed 300 mm away from the center of the notch location to give angles of the incident wave of 0°, 45° and 90° relative to the normal of the notch (Fig. 2). The transducers consist of a PZT disc (Ferroperm Pz27, diameter 5 mm, thickness 2 mm) and a brass backing mass (height 6 mm) and were permanently bonded to the plate using two-component epoxy glue. The transducers act in good approximation as point sources for the excitation of the first antisymmetric Lamb wave mode A_0 .

The excitation signal was a 5 cycle toneburst with a center frequency of 100 kHz modulated by a Hanning window. The signal was generated in a programmable function generator and amplified using a power amplifier. The velocity of the out-of-plane displacement was measured using a laser interferometer every 5 degrees on a circle around the notch with a radius of 30 mm. The full time traces of the measured signals were bandpass filtered (75 kHz – 125 kHz), averaged and recorded in a digital storage oscilloscope. Similar to the FE simulations, an initial measurement was done for each excitation transducer before the milling of the notch to capture the incident wave field, and then for each notch depth. The measured time traces were time gated and the amplitude and phase (complex magnitude) at 100 kHz determined using FFT. Due to the re-positioning of the plate after each milling step relative to the laser, the repeatability was limited to a noise level of about 5% of the amplitude of the incident wave when taking the difference between complex magnitudes to evaluate the scattered field. The amplitudes were normalized with the amplitude of the incident wave.

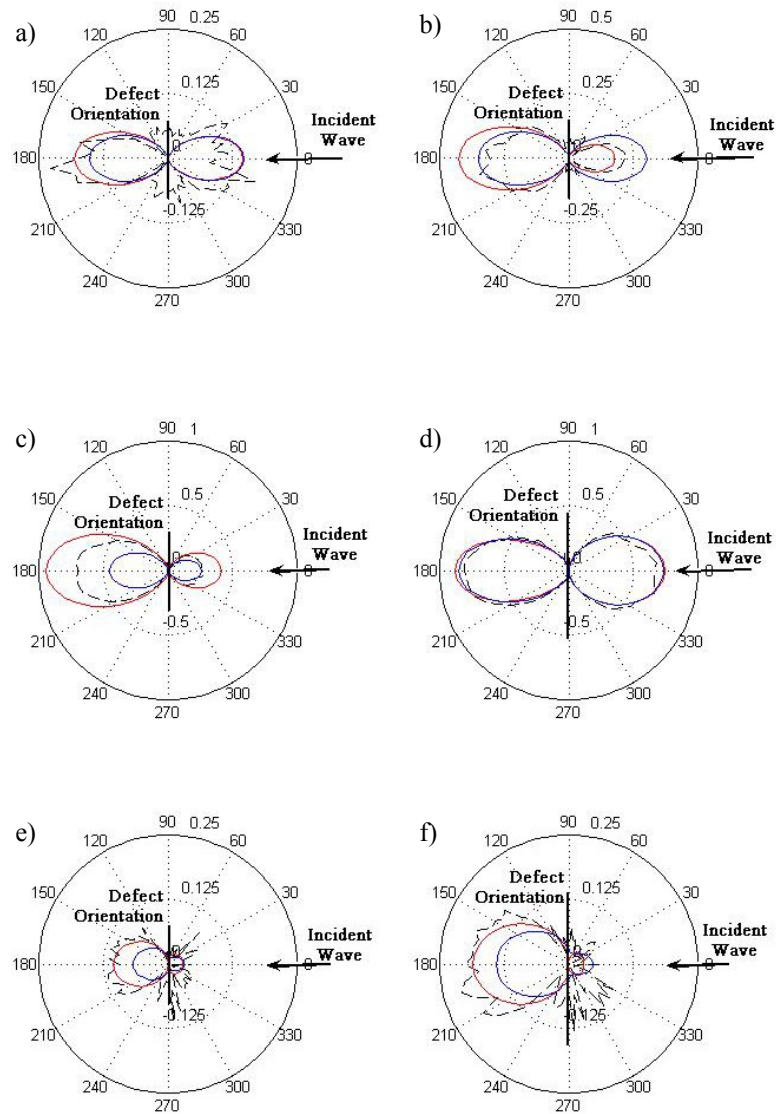


Fig. 3. Polar plot of normalized amplitude of A_0 mode scattered at defect (monitored at 30 mm radius); orientation 90° - 270° ; incident wave from 0° ; $f = 100$ kHz; $\lambda = 19$ mm; experiment notch (black, dashed), simulation notch (red, solid), simulation crack (blue, solid): a) $a = 20$ mm, $\frac{1}{4}$ thickness; b) $a = 20$ mm, $\frac{1}{2}$ thickness; c) $a = 20$ mm, $\frac{3}{4}$ thickness; d) $a = 20$ mm, through thickness; e) $a = 5$ mm, $\frac{1}{4}$ thickness; f) $a = 5$ mm, through thickness.

4. COMPARISON OF ANGULAR SCATTERING PATTERN

The polar plots of the amplitude patterns from experiments and FE simulations for an incident wave perpendicular to the defect orientation (0° direction) are shown in Fig. 3. For this incident wave direction, the scattering pattern is symmetric, with a back-scattered lobe in the 0° direction and a shadow area in the 180° direction. The defect blocks the incident wave path, reflecting some of the energy and amplitude reduction occurs. From the scattering patterns it is clear that almost no scattering occurs along the defect orientation, i.e., in the 90° and 270° directions. For a long (20 mm length, approximately λ) and shallow ($\frac{1}{4}$ plate depth) defect (Fig. 3a), the amplitude of both the back and forward scattered wave lobes are rather small. Due to the 5% error from plate repositioning, an irregular pattern for the experimental curve can be observed. With increasing defect depth, initially the amplitude of the forward scattered lobe (shadow area) increases and an increased backscattered wave is observed for a long and deep (through thickness, Fig. 3d) defect. For the case of a short (5 mm length, approximately $\lambda/4$) and shallow ($\frac{1}{4}$ & $\frac{1}{2}$ depth) defect, the predicted scattered amplitude is very small and almost no experimental scattering could be observed (not shown). With increasing defect

depth, a forward scattered wave can be seen, with good agreement between measurements and simulations (Fig. 3e/f). In contrast to the results for a long defect, only a forward scattered wave due to the blocking of the wave path can be seen, with very limited scattered amplitude in all other directions, including the backscattered direction (0°).

Good agreement of the measured and simulated amplitude patterns can be observed, helping to validate the FE simulations. Distinct scattering amplitude patterns could be observed, which should be considered for the prediction of defect detection sensitivity using guided wave arrays [20]. Almost no scattered wave was observed along the defect orientation. For shallow and short defects, mostly a shadow area behind the defect with reduced amplitude due to the blocking of the wave path was found. Large backscattered wave amplitude was mostly observed for defects that are deep and long compared to the wavelength of the incident wave.

5. FINITE ELEMENT CALCULATION OF SCATTERED AMPLITUDE

The FE simulations were used to predict the scattered amplitude patterns for a variation of the geometrical parameters. Figure 4 shows the FE predictions of maximum scattered amplitude for a through thickness and half thickness defect with increasing length and two incident wave directions. For the case of a through thickness defect (Fig. 4a/b), the amplitude increases with defect length and significant scattered waves with similar amplitudes to the incident wave are predicted. It should be noted that the amplitude does not increase linearly with defect length, but that a stepped pattern, especially for the 45° incident wave direction (Fig. 4b), can be observed. This occurs at approximately half wavelength (10 mm defect length) and wavelength and correlates to observed changes in the angular scattering pattern. For the case of a defect half through the plate thickness, lower scattered amplitude but a mostly linear increase with defect length can be seen in Fig. 4c/d. Low scattered amplitude for short, part-thickness defects would make long-range detection difficult, but for longer defects scattered amplitudes comparable to approximately half the incident wave amplitude are predicted.

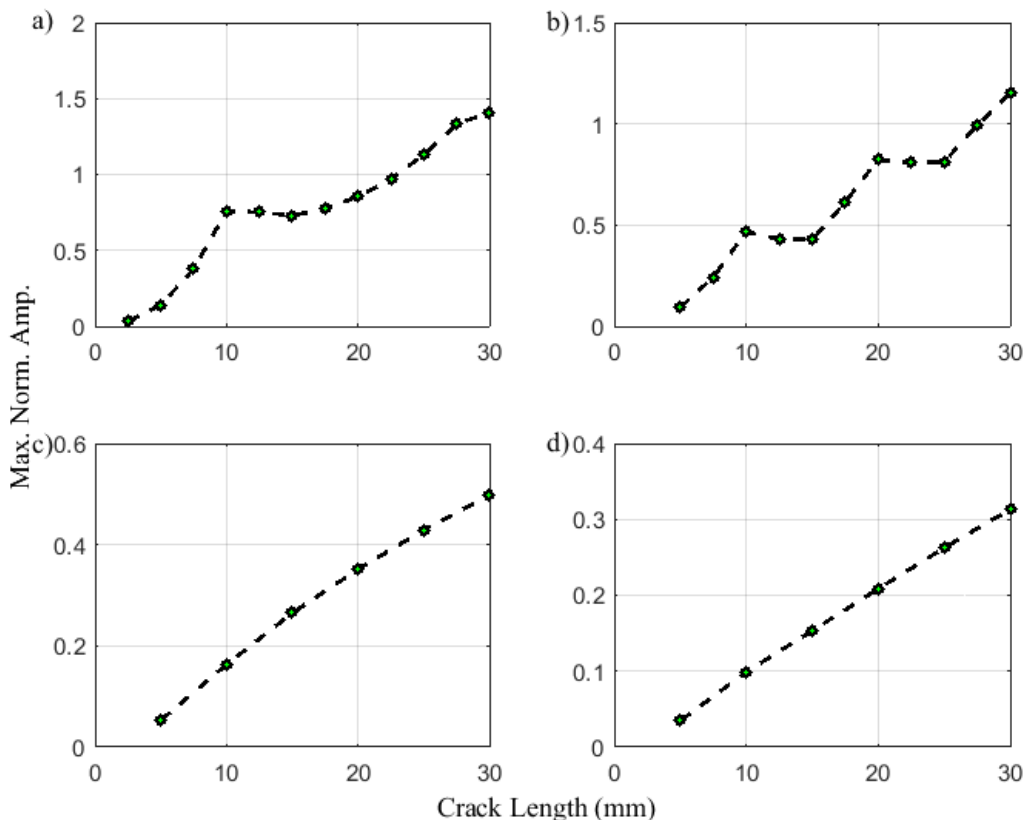


Fig. 4. Maximum scattered amplitude of A_0 mode (monitored at 30 mm radius) for variation of defect length; $f = 100$ kHz; $\lambda = 19$ mm: a) defect through thickness, incident wave from 0° direction (perpendicular); b) defect through thickness, incident wave from 45° direction; c) defect half thickness, incident wave from 0° direction (perpendicular); d) defect half thickness, incident wave from 45° direction.

6. CONCLUSIONS

The scattering of the A_0 Lamb wave mode at part-through and through thickness notches defects in aluminum plates was measured experimentally and predicted from FE simulations. Good agreement of the scattered field directivity patterns and amplitudes was found. For small scattered amplitudes, the sensitivity of the measurements is limited due to noise in the baseline subtraction introduced by the repositioning of the plate. Almost no scattered wave was observed along the defect orientation. For shallow and short defects, mostly a shadow area behind the defect with reduced amplitude due to the blocking of the wave path was found. Large backscattered wave amplitude was mostly observed for defects that are deep and long compared to the wavelength of the incident wave. The FE simulations predict a significant increase in the scattered wave amplitude for long defects and for the case of the incident wave mostly perpendicular to the defect orientation. These results can be employed for the development of permanently attached guided wave arrays for SHM.

REFERENCES

- [1] Michaels, J.E., Michaels, T.E. and Mi, B., "An ultrasonic angle beam method for in situ sizing of fastener hole cracks," *J. Nondestruct. Eval.* 25, 3-16 (2006).
- [2] Castaigns, M., Le Clezio, E. and Hosten, B., "Modal decomposition method for modeling the interaction of Lamb waves with cracks," *J. Acoust. Soc. Am.* 112, 2567-2582 (2002).
- [3] Rose, J.L., "Standing on the shoulders of giants: An example of guided wave inspection," *Mat. Eval.* 60, 53-59 (2002).
- [4] Fan, Z., Castaigns, M., Lowe, M.J.S., Biateau, C. and Fromme, P., "Feature-guided waves for monitoring adhesive shear modulus in bonded stiffeners," *NDT&E Int.* 54, 96-102 (2013).
- [5] Masserey, B. and Fromme, P., "Fatigue Crack Growth Monitoring using High Frequency Guided Waves," *Struct. Health Monit.* 12, 484-493 (2013).
- [6] Masserey, B. and Fromme, P., "In-Situ Monitoring of Fatigue Crack Growth using High Frequency Guided Waves," *NDT&E Int.* 71, 1-7 (2015).
- [7] Chan, H., Masserey B. and Fromme, P., "High frequency guided ultrasonic waves for hidden fatigue crack growth monitoring in multi-layer model aerospace structures," *Smart Mater. Struct.* 24, 025037 (2015).
- [8] Masserey, B., Raemy, C. and Fromme, P., "High-frequency guided ultrasonic waves for hidden defect detection in multi-layered aircraft structures," *Ultrasonics* 54, 1720-1728 (2014).
- [9] Fromme, P., Wilcox, P.D., Lowe, M.J.S. and Cawley, P., "On the development and testing of a guided ultrasonic wave array for structural integrity monitoring," *IEEE Trans. Ultrason. Ferroelectr. Freq. Control* 53, 777-785 (2006).
- [10] Croxford, A.J., Wilcox, P.D., Drinkwater, B.W. and Konstantinidis, G., "Strategies for guided-wave structural health monitoring," *Proc. Roy. Soc. A* 463, 2961-2981 (2007).
- [11] Michaels, J.E. and Michaels, T.E., "Guided wave signal processing and image fusion for in situ damage localization in plates," *Wave Motion* 44, 482-492 (2007).
- [12] Fromme, P., "Monitoring of Plate Structures Using Guided Ultrasonic Waves," *AIP Conf. Proc.* 975, 78-85 (2008).
- [13] Hall, J.S., Fromme, P. and Michaels, J.E., "Guided Wave Damage Characterization via Minimum Variance Imaging with a Distributed Array of Ultrasonic Sensors," *J. Nondestruct. Eval.* 33, 299-308 (2014).
- [14] Lowe, M.J.S., Cawley, P., Kao, J.Y. and Diligent, O., "The low frequency reflection characteristics of the fundamental antisymmetric Lamb wave a_0 from a rectangular notch in a plate," *J. Acoust. Soc. Am.* 112, 2612-2622 (2002).
- [15] Pao, Y.H. and Chao, C.C., "Diffractions of flexural waves by a cavity in an elastic plate," *AIAA J.* 2, 2004-2010 (1964).
- [16] Fromme, P. and Sayir, M.B., "Measurement of the scattering of a Lamb wave by a through hole in a plate," *J. Acoust. Soc. Am.* 111, 1165-1170 (2002).
- [17] Diligent, O., Grahn, T., Bostrom, A., Cawley, P. and Lowe, M.J.S., "The low-frequency reflection and scattering of the S_0 Lamb wave mode from a circular through-thickness hole in a plate: Finite Element, analytical and experimental studies," *J. Acoust. Soc. Am.* 112, 2589-2601 (2002).
- [18] Fromme, P. and Sayir, M.B., "Detection of cracks at rivet holes using guided waves," *Ultrasonics* 40, 199-203 (2002).
- [19] Rouge, C. and Fromme, P., "Directivity of guided ultrasonic wave scattering at notches and cracks," *J. Phys.: Conf. Ser.* 269, 012018 (2011).
- [20] Fromme, P., "Health Monitoring of Plate Structures Using Guided Waves," *Proc. of SPIE* 6935, W9350 (2008).